Industrial Crops and Products 42 (2013) 480–488

Contents lists available at SciVerse ScienceDirect

Industrial Crops and Products

journal homepage: www.elsevier.com/locate/indcrop

Extraction and characterization of cellulose nanocrystals from agro-industrial residue – Soy hulls

Wilson Pires Flauzino Neto[a], Hudson Alves Silvério[a], Noélio Oliveira Dantas[b], Daniel Pasquini[a,*]

[a] Instituto de Química, Universidade Federal de Uberlândia, Campus Santa Mônica, Av. João Naves de Ávila, 2121, 38400-902 Uberlândia, Minas Gerais, Brazil
[b] Instituto de Física, Universidade Federal de Uberlândia, Campus Santa Mônica, Av. João Naves de Ávila, 2121, 38400-902 Uberlândia, Minas Gerais, Brazil

ARTICLE INFO

Article history:
Received 24 April 2012
Received in revised form 14 June 2012
Accepted 26 June 2012

Keywords:
Cellulose nanocrystals
Soy hulls
Agro-industrial residue
Reinforcement
Nanocomposites

ABSTRACT

Soy hulls are an agro-industrial residue available in huge quantities throughout the world whose application deserves more attention than simply as cattle feed. This work evaluates the use of soy hulls as a source of cellulose to obtain nanocrystals by acid hydrolysis. The hydrolysis was performed at 40 °C for 30 or 40 min, using 30 mL of H_2SO_4 64% for each gram of cellulose. The resulting nanocrystals were characterized by crystallinity index, morphology, surface charge and thermal stability. The results showed that the more drastic hydrolysis conditions (40 min) resulted in a shorter length of nanocrystals and caused some damage on the crystalline structure of the cellulose. At an extraction time of 30 min, the nanocrystals presented a high crystallinity (73.5%), an average length of 122.66 ± 39.40 nm, a diameter of 2.77 ± 0.67 nm and an aspect ratio around 44, therefore presenting a great potential as reinforcement in nanocomposite preparations.

1. Introduction

Given the problems involved in plastic recycling and the dwindling exhaustion of fossil resources, there is a great interest in sustainable and environmentally friendly materials. As a result, in recent years, the development of biopolymers for applications in which synthetic polymers or mineral fillers are traditionally used, has been the object of intensive academic and industrial research (Angellier et al., 2005). In this context, the application of cellulose nanocrystals (CWs) as reinforcement in polymer matrixes has attracted considerable attention in this field since it offers a unique combination of high physical properties and environmental benefits (Habibi et al., 2010; Peng et al., 2011). CWs based nanocomposites generally exhibit significant improvements in thermal, mechanical, and barrier properties compared to the neat polymer or conventional composites (Azeredo et al., 2009).

Cellulose nanocrystals are needle-shaped cellulose particles with at least one dimension equal or less than 100 nm and have a highly crystalline nature (almost defect-free crystallites). In the literature, there are different terms to denominate these nanoparticles, e.g. cellulose nanowhiskers, cellulose whiskers, cellulose crystallites, cellulose crystals, cellulose nanocrystals, nanocrystalline cellulose, cellulose monocrystals and cellulose microcrystals (Lima and Borsali, 2004; Peng et al., 2011; Shi et al., 2011).

The main features that stimulate the use of CWs as polymer reinforcement agents are their large specific surface area (estimated to be several hundreds of $m^2\,g^{-1}$), their very high modulus of elasticity (approximately 150 GPa), their great aspect ratio, and their ability to act as a significant reinforcement at low filler loading levels. Other attractive advantages of CWs are their low density (about 1.566 g/cm^3), non-abrasive nature, non-toxic character, biocompatibility and biodegradability. Additionally, the CWs come from renewable natural sources which are very abundant and therefore low-costing, it is not necessary to synthesize them, and they allow the production of composites films with excellent visible light transmittance which are easily modified chemically (their structure has a reactive surface of –OH side groups that facilitate grafting chemical species to achieve different surface properties) (Moon et al., 2011; Peng et al., 2011).

Among the several methods for preparing cellulose nanostructures, the acid hydrolysis is the most well-known and widely used (Peng et al., 2011). This process breaks the disordered and amorphous parts of the cellulose, releasing single and well-defined crystals. Thus, this procedure to isolate CWs is based on the quicker hydrolysis kinetics presented by the amorphous regions, as compared to the crystalline ones (Habibi et al., 2010; Peng et al., 2011; Teixeira et al., 2011).

Regarding extraction by acid hydrolysis, the temperature and the time of reaction, acid nature, acid concentration and the acid-to-cellulose ratio are also important parameters that affect the

* Corresponding author. Tel.: +55 34 3239 4143; fax: +55 34 3239 4208.
E-mail addresses: danielpasquini2005@yahoo.com.br, pasquini@iqufu.ufu.br (D. Pasquini).

0926-6690/$ – see front matter © 2012 Elsevier B.V. All rights reserved.
http://dx.doi.org/10.1016/j.indcrop.2012.06.041

morphology and properties of CWs (Habibi et al., 2010; Peng et al., 2011; Teixeira et al., 2011).

It is known that the morphology and properties of the CWs influence their performance as a reinforcing agent (Eichhorn et al., 2010). It is also known that the morphology and properties of the CWs depend main on the source of the original cellulose and the extraction process (Moon et al., 2011; Peng et al., 2011). Therefore, the performance of the CWs as reinforcing particles is dependent on the source of the original cellulose. Thus, the development of CWs from different resources of cellulose is relevant.

Soy is one of the main agricultural products in the world. Brazil stands as the second largest producer of soybeans, accounting for 28% of the world production (http://www.cnpso.embrapa.br/index.php?cod_pai=2&op_page=294). The oil and protein constituents of soybeans are the main income generators in soy plants and consequently little attention is paid to the applications of soy hulls (Alemdar and Sain, 2008). Soy hulls are obtained in the soybean oil extraction process since it is necessary to remove the film coating the grain for the oil extraction. For each ton of soy seed processed, about 2% of the total mass matches the by-product in question (Zambom et al., 2001). At present, some soy hulls are used as a fiber source for cattle, however, huge amounts of soy hulls are left to waste (Alemdar and Sain, 2008; Ipharraguerre and Clark, 2003).

Soy hulls are an agro-industrial waste available in huge quantities in many countries, including Brazil, which deserves to be used in other different applications. Although there is not yet any published work on the extraction of CWs from soy hulls fiber, in the literature can be found papers on extraction of cellulose nanofibers from soy hulls and soybean pod (another residue generated from the soy crop activity) (Alemdar and Sain, 2008; Wang and Sain, 2007).

The use of biomass residues for projects other than feedstock, such as in the production of high performance materials, is a prospective commercial application that would unlock the potential for a generation of value-added products from agro-industrial commodities (Alemdar and Sain, 2008; Purkait et al., 2011). Various cellulosic resources have been used by researchers to generate CWs, but the use of agro-waste as a precursor is very rare (Purkait et al., 2011).

In the present paper, CWs were extracted and characterized from soy hulls by acid hydrolysis in order to evaluate their suitability as a reinforcement agent for the manufacture of nanocomposites. Different techniques were employed to characterize the fibers and cellulose nanocrystals of soy hulls in order to investigate the chemical composition, crystallinity index, thermal stability, surface charge and morphology (shape and size).

2. Materials and methods

The soy hulls were supplied by Algar Agro S. A. (Uberlândia, Minas Gerais, Brazil). The other reagents employed in this study were: sulfuric acid (95.0–98.0 wt%, Vetec, P.A.), sodium hydroxide (Vetec), potassium hydroxide (Vetec), sodium chlorite ($NaClO_2$, technical grade, 80%, Sigma–Aldrich), glacial acetic acid (Synth), and cellulose membrane (D9402, Sigma–Aldrich).

2.1. Purification

Initially the soy hulls (SH) were treated with a sodium hydroxide aqueous solution of 2% (w/w) for 4 h at 100 °C under mechanical stirring and then washed several times with distilled water until the alkali was completely removed, and finally dried at 50 °C for 12 h in an air-circulating oven. After this treatment, the fibers were bleached with a solution made up of equal parts (v:v) of acetate buffer (27 g NaOH and 75 mL glacial acetic acid, diluted to 1 L of distilled water) and aqueous sodium chlorite (1.7 wt% $NaClO_2$ in water). This bleaching treatment was performed at 80 °C for 4 h. The bleached fibers were washed repeatedly in distilled water until the pH of the fibers became neutral and subsequently dried at 50 °C for 12 h in an air-circulating oven. The fiber content throughout these chemical treatments was about 4–6% (w/w) (de Rodriguez et al., 2006; Siqueira et al., 2010). The material which resulted after the purification was the treated soy hulls (TSH).

2.2. Extraction of cellulose nanocrystals

After the chemical treatment was completed, the TSH were milled with a blender and passed through a 35-mesh screen and then used for the extraction of nanocrystals by acid hydrolysis. The hydrolysis was performed at 40 °C for 30 min or 40 min under vigorous and constant stirring. For each gram of TSH we used 30 mL of H_2SO_4 64% (w/w). Immediately following the hydrolysis, the suspension was diluted 10-fold with cold water to stop the hydrolysis reaction, and centrifuged twice for 10 min at 7000 rpm to remove the excess acid. The precipitate was then dialyzed with tap water to remove non-reactive sulfate groups, salts and soluble sugars, until the neutral pH (5–7 days) be reached. Subsequently, the resulting suspension of dialysis process was treated using a disperser type UltraTurrax for 5 min at 20,000 rpm and sonicated for 5 min. The colloidal suspension was stored in a refrigerator at 4 °C with the addition of some drops of chloroform to avoid any bacterial growth. The cellulose nanocrystals or whiskers of soy hulls were labeled WSH_{30} or WSH_{40} depending on the time of extraction.

2.3. Gravimetric analysis

The hydrolysis yield and the WSH concentration in the final suspension were calculated drying an aliquot of the suspension with a known volume at 105 °C for 12 h in an air-circulating oven.

2.4. Chemical composition

The chemical composition of SH and TSH was measured as follows. The lignin content was determined according to a standard method of Technical Association of Pulp and Paper Industry TAPPI T222 om-88. The holocellulose (α-cellulose + hemicellulose) content was estimated by the acid chlorite method (Browning, 1967). The α-cellulose content was determined treating the holocellulose with potassium hydroxide solutions (Browning, 1967). The hemicellulose content was found by subtracting the α-cellulose part from the holocellulose content. An average of three replicates was calculated for each sample.

2.5. Fourier transform infrared spectroscopy (FTIR)

A Shimadzu IRPrestige-21 infrared spectrophotometer was used to obtain spectra for the SH, TSH and WSH_{30}. The KBr disk (ultrathin pellets) method was used in taking the IR spectra. Samples were ground and mixed with KBr (sample/KBr ratio, 1/100) to prepare pastilles. The experiments were carried out using in the range of 400–4000 cm^{-1} with a resolution of 4 cm^{-1} and a total of 32 scans for each sample.

2.6. Elemental analysis

Elemental analysis was performed mainly to determine the total sulfur content before and after the extraction of nanocrystals. It was carried out with an EA1110-CHNS/O elemental analyzer from CE Instruments.

2.7. X-ray diffraction (XRD)

The X-ray diffractograms of SH, CSH, WSH_{30} and WSH_{40} were obtained at room temperature within a 2θ range from 5 to 40° and a scan rate of 1° min^{-1}. The equipment used was a diffractometer Shimadzu LabX XRD-6000, operating at a power of 40 kV with a current of 30 mA and Cu Kα radiation (1.5406 Å). Before performing the XRD, all samples were dried at 50 °C for 12 h in an air-circulating oven. The crystallinity index (CrI) of the material was determined by the Segal method (Segal, 1959) as shown in Eq. (1):

$$\mathrm{CrI} = \left[\frac{(I_{002} - I_{\mathrm{am}})}{I_{002}}\right] \times 100 \quad (1)$$

In this equation, CrI expresses the relative degree of crystallinity, I_{002} is the intensity of the 0 0 2 lattice diffraction at $2\theta = 22.8°$, and I_{am} is the intensity of diffraction at $2\theta = 18°$. I_{002} represents both crystalline and amorphous regions while I_{am} represents only the amorphous part.

The average thickness of cellulose crystallites was estimated from the X-ray diffraction patterns by using Scherrer's Eq. (2) (Klug and Alexander, 1974):

$$D_{hkl} = \frac{K\lambda}{\beta_{1/2}\,\mathrm{Cos}\,\theta} \quad (2)$$

where D_{hkl} is the crystallite dimension in the direction normal to the $h\,k\,l$ family of lattice planes, K is the correction factor and usually taken to be 0.9, λ is the radiation wavelength, θ is the diffraction angle and $\beta_{1/2}$ is the peak width at half maximum intensity. The crystal size was determined perpendicular to the 0 0 2 planes. Before plotting, data were smoothed over 35 adjacent points and then normalized, so that the main peaks had the same y-axis values and could be compared directly.

2.8. Scanning electron microscopy (SEM)

The morphology of TSH was evaluated by SEM on a JEOL JSM-7500F microscope. A sample was coated with a 1–10-nm-thick carbon layer and then observed with an accelerating voltage of 2–10 kV.

2.9. Transmission electron microscopy (TEM)

The morphology of WSH_{30} and WSH_{40} were examined by TEM in a Zeiss EM 109 transmission electron microscope equipped with a system for digital image capture Olympus MegaView V. A drop of diluted nanocrystals aqueous suspension was deposited on a Cu microgrid (200 mesh) and allowed to dry. The grid was negatively stained with a 3% (w/w) solution of uranyl acetate and dried at room temperature. The sample was observed at 80 kV. The dimensions of whiskers were determined using digital image analyses (ImageJ). A hundred nanocrystals were randomly selected and a minimum of 100 and 200 measurements were used to determine the average length and the diameter, respectively.

2.10. Atomic force microscopy (AFM)

The AFM measurements were performed with Shimadzu SPM-9600 equipment for evaluating the thickness of the WSH_{30}. A drop of diluted nanocrystals aqueous suspension was deposited onto a freshly cleaved mica surface and air-dried. AFM images were obtained at room temperature in the dynamic mode with a scan rate of 1 Hz and using Si tips with a curvature radius of less than 10 nm and a spring constant of 42 N m^{-1}. The thicknesses of nanocrystals were determined using the VectorScan software (software for Shimadzu's SPM-9600). To eliminate the effect of tip radius on width measurements, we measured the heights of the nanocrystals, which are not subject to peak broadening artifacts, and assumed the nanocrystals to be cylindrical in shape (Beck-Candanedo et al., 2005). A hundred nanocrystals were randomly selected and two measurements for each nanocrystal were used to determine the average thickness.

Fig. 1. Images of soy hulls before (left) and after the purification (right).

2.11. Thermal characterization

Thermal stabilities of SH, TSH and WSH_{30} were evaluated using Shimadzu DTG-60H equipment. The analysis conditions were: a nitrogen atmosphere with flow 30 mL min^{-1}, heating rate of 10 °C min^{-1}, temperature range 25–600 °C, sample mass between 5 and 7 mg and aluminum pans.

3. Results and discussion

3.1. Purification and chemical composition

A diluted alkali treatment was performed to solubilize the lignin, pectins, hemicelluloses and proteins (Dufresne et al., 1997), while the bleaching was applied to remove the lignin residues (de Rodriguez et al., 2006). The yield of purification was 46% (by dry mass). Fig. 1 shows the physical aspect of the SH before and after purification (TSH). Visually, a white colored TSH was obtained, indicating that a great part of the initial non-cellulosic components were removed by purification process, consequently TSH have higher cellulose content than SH.

The contents of the cellulose were 48.2 ± 2.1% and 84.6 ± 4.0%, of the hemicelluloses were 24.0 ± 3.0% and 11.2 ± 4.0%, and lignin were 5.78 ± 1.06% and 3.67 ± 0.33%, for SH and TSH, respectively. The values found for the main constituents of SH are in agreement with literature data (Ipharraguerre and Clark, 2003; Zambom et al., 2001).

The sum of the percentage of cellulose, hemicelluloses and lignin to the SH corresponds to 78.0% of the total dry matter, showing that there are other components in SH (e.g. protein, extractives and ash). As showed above, after the purification, the cellulose content significantly increased, while the hemicelluloses content was reduced to approximately half of the original, and the lignin content was reduced to approximately two-third of the original.

The sum of the percentage of cellulose, hemicelluloses and lignin to the TSH corresponds to 99.5% of the total dry matter, therefore the purification not only removed hemicelluloses and lignin but also other components such as proteins, extractives and ash. The purification process was effective so the composition of TSH is suitable for the extraction of whiskers. It was verified that the percentage of mass consumption of the main components of the SH due to the purification process was 19.3, 78.3 and 56.0% for α-cellulose, hemicelluloses and lignin, respectively. The mass loss of

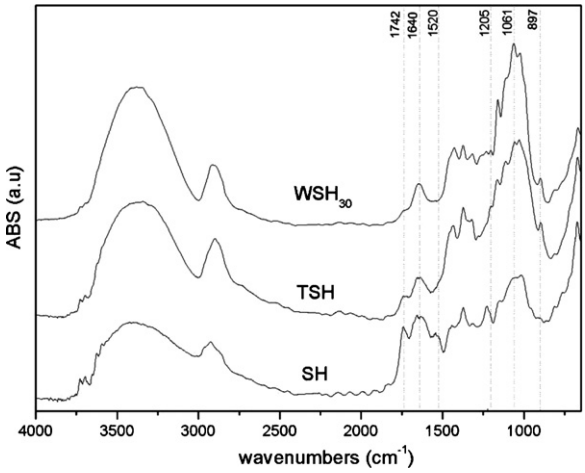

Fig. 2. FTIR spectra of untreated soy hulls (SH), treated soy hulls (TSH) and cellulose nanocrystals of soy hulls obtained by acid hydrolysis of 30 min (WSH_{30}).

cellulose during the purification process can be related to two factors: (i) the breakdown of cellulose chains during bleaching and (ii) the loss of material inherent in various filtering processes and mass transfer.

Fig. 2 shows the FTIR spectra of SH, TSH and WSH_{30}. The peak at 1742 cm^{-1} in the spectrum of SH is attributed to the acetyl and uronic ester groups of hemicellulose or the ester linkage of carboxylic group of ferulic and p-coumaric acids of lignin and/or hemicelluloses (Sun et al., 2005). This peak decreased in the spectrum of TSH due to the significant removal of hemicelluloses and lignin, and finally almost disappeared in the spectra of WSH_{30} because of acid extraction.

The peak at 1640 cm^{-1} is assigned to the absorbed water. Although the peak at 1630 cm^{-1} in SH and TSH may be from the water, we believe that it was predominantly attributed to the aromatic C=C stretch of aromatic ring in the lignin (Sun et al., 2005). The contribution from the absorbed water predominates in the case of WSH_{30}.

The broad peak at 1520 cm^{-1} in the spectra of SH and TSH are indicative of the presence of lignin and attributed to the C=C vibration (Sun et al., 2005). This peak disappeared in WSH_{30}, further indicating the removal of the corresponding groups from lignin. The tiny peak at 1205 cm^{-1} in the spectra of WSH_{30} is related to S=O vibration, due the esterification reaction, as reported in previous literature (Lu and Hsieh, 2010).

The peaks at 1061 and 897 cm^{-1} are associated with cellulose the C–O stretching and C–H rock vibrations of cellulose (Alemdar and Sain, 2008), which appeared in all of the spectra. The growth of these peaks showed the increase in the percentage of cellulosic components. The differences in the spectra of TSH and WSH_{30} indicate that these samples have higher cellulose content, suggesting that they are almost pure cellulose.

3.2. Extraction of cellulose nanocrystals and elemental analysis

The yields of the WSH, with respect to the initial amount of dried TSH fibers, for WSH_{30} and WSH_{40} were 20 and 8 wt%, respectively; these values were similar to those found to sesame husk nanocrystals (Purkait et al., 2011). The concentration of the final suspensions of WSH_{30} and WSH_{40} were 2.3431 and 0.9198 g L^{-1}, respectively. The lower concentration of WSH_{40} suspension with respect to WSH_{30} gave an initial evidence of cellulose degradation using 40 min for acid hydrolysis.

Elemental analysis revealed that the concentration of negatively charged sulfate groups in TSH, WSH_{30} and WSH_{40} are

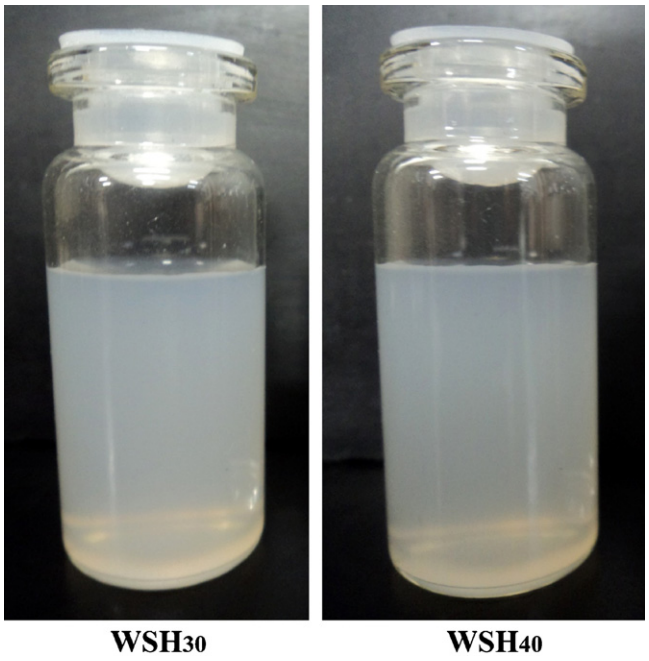

Fig. 3. The resulting colloidal suspensions for WSH_{30} and WSH_{40}.

0, 118 and 111 mmol SO_4^- kg^{-1} of cellulose, respectively. The se results confirm the incorporation of sulfate groups into the cellulose chains after acid treatment and also that both hydrolysis conditions used led to obtaining homogeneous and stable aqueous suspensions (as can be seen in Fig. 3). It is known that the increase of extraction time results in higher sulfate content in the CWs, however, the sulfate content was higher for WSH_{30} than for WSH_{40}. Probably, this unexpected behavior is associated with the lack of a strict control of the dialysis time, since the dialysis promotes the desulfation on the nanocrystals surfaces (Wang et al., 2007). The presence of the sulfate groups in WSH_{30} was also confirmed by the FTIR, as showed in Fig. 2 and discussed earlier.

3.3. X-ray diffraction

The X-ray diffraction patterns of SH, TSH, WSH_{30} and WSH_{40} are shown in Fig. 4. These patterns are typical of semicrystalline

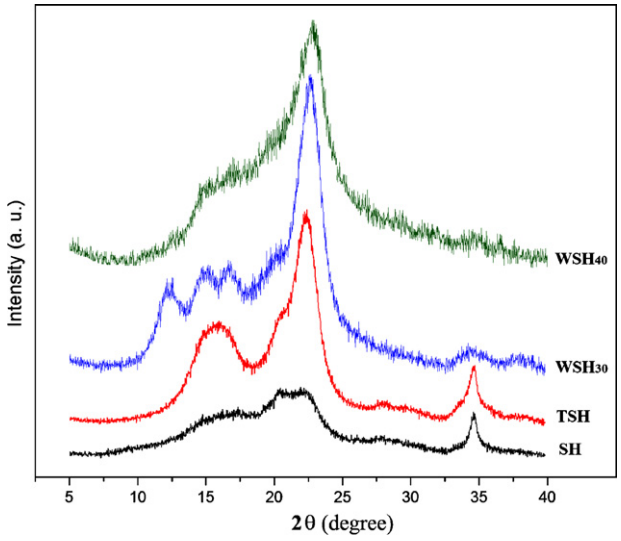

Fig. 4. X-ray diffractograms of SH, TSH, WSH_{30} and WSH_{40}.

materials with an amorphous broad hump and crystalline peaks. From these data, the CrI was determined using the procedure described in Section 2. By this method, the CrI was found to be about 26.3, 67.2, 73.5 and 64.4% for the SH, TSH, WSH_{30} and WSH_{40}, respectively.

The higher CrI value of TSH compared to SH can be well understood by the reduction and removal of amorphous non-cellulosic compounds induced by the alkali and bleaching treatments performed in the purification process. The increase in CrI value of WSH_{30} in relation to TSH was also observed, due to the partial removal of the para-crystalline domains during the acid hydrolysis. In Fig. 4, narrower and sharper peaks for WSH_{30}, can be observed because of their higher crystallinity compared to other samples.

A decrease in CrI of WSH_{40} with respect to WSH_{30} and TSH was observed, and this suggests that the extraction time of 40 min was severe under the hydrolysis conditions employed, therefore the acid treatment of 40 min not only removed the amorphous portion of cellulose but also partly destroyed the crystalline ones. A similar effect of a hydrolysis time in excess was observed in a previous study (Teixeira et al., 2011; Chen et al., 2009).

In all diffractograms profiles (Fig. 4), there is a predominance of type I cellulose, verified by the presence of peaks at $2\theta = 15^\circ$ (plane 1 0 1), 17° (plan 1 0 $\bar{1}$), 21° (plane 0 2 1), 23° (plane 0 0 2) and 34° (plane 0 0 4), though the diffraction patterns of WSH_{30} and WSH_{40} display a mixture of polymorphs of cellulose I and cellulose II. The presence of cellulose type II can be observed by peaks at $2\theta = 12^\circ$ (plane 1 0 1), 20° (plan 1 0 $\bar{1}$) and 22° (plane 0 0 2) (Borysiak and Garbarczyk, 2003).

Possibly the presence of cellulose type II is associated to the re-precipitation of cellulose after hydrolysis, since a 64% sulfuric acid solution can be a solvent for cellulose. The samples of WSH should have about the same amount of cellulose type II, however, the sample WSH_{40} (that has the higher extraction time) practically presents no cellulose type II content in your diffractogram profile; due to the fact that type II cellulose is more susceptible to hydrolysis than native cellulose (Xiang et al., 2003).

The average cross-sectional dimension of the elementary cellulose crystallites was determined from X-ray diffractograms by applying Scherrer's expression as described in Section 2. Since Scherrer's equation is restricted to samples of high crystallinity and without any broadening of peaks, this calculation was made only for WSH_{30} and the value found was 2.73 nm.

3.4. Microscopic analyses

3.4.1. Scanning electron microscopy (SEM)

The SEM picture of TSH was taken to investigate their structure and is shown in Fig. 5. Visually, it is clear that TSH is a micro-sized fiber that exhibited an irregular shape and size (about 14–125 μm in length and 4–15 μm in width).

3.4.2. Transmission electron microscopy (TEM) and atomic force microscopy (AFM)

Fig. 6 shows TEM micrographs of cellulose whiskers extracted for WSH_{30} and WSH_{40}. TEM pictures presented needle-like nanoparticles, confirming that the extraction of whiskers from soy hulls was successful. These images show individual nanocrystals and some aggregates. The appearance of laterally aggregated elementary crystallites in TEM images is expected due to the high specific area and strong hydrogen bonds established between the whiskers. These aggregates may exist even in suspension but, when the dispersing medium is removed, as in the case of the TEM sample preparation, bundles of whiskers can be even more numerous than individualized needle (Elazzouzi-Hafraoui et al., 2008).

Fig. 7 shows the length (L), width (D) and aspect ratio (L/D) distributions of WSH obtained by several TEM images, as described in Section 2. The statistics of the WSH length, width and aspect ratio are shown in Table 1.

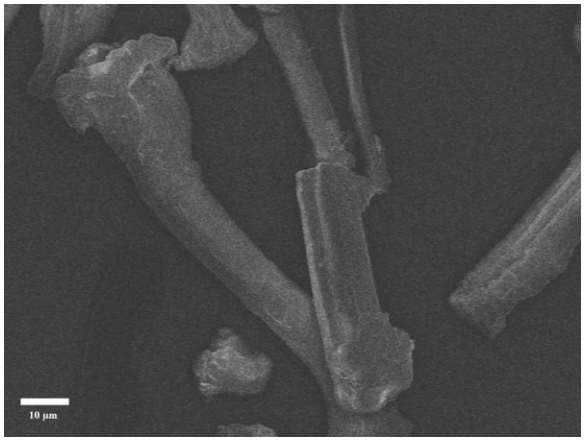

Fig. 5. SEM image of TSH (magnification: 1000×).

The increase in extraction time resulted in a slight shorter length for WSH_{40} when compared with WSH_{30}. This was expected, since the long extraction time (40 min) partially destroyed areas of the crystalline domains as seen by XRD analysis. No significant difference in diameter among the whiskers could be detected by TEM, if the standard deviation of each value is taken into account. With increasing hydrolysis time, the standard deviation of the dimensions distribution decreased (see Table 1) (Elazzouzi-Hafraoui et al., 2008).

As a consequence of the whiskers preparation conditions, a decrease in the aspect ratio (L/D) of WSH_{40} compared with WSH_{30} was observed by TEM measurements. This suggests that WSH_{30} can give a better reinforcing effect than WSH_{40} at the same filler loading levels (Eichhorn et al., 2010). The aspect ratio of the WSH from TEM images were higher than 10, considered as the minimum value for a good stress transfer from the matrix to the fibers for any significant reinforcement to occur (Azeredo et al., 2009). As seen in Fig. 6 it was difficult to clearly discern individual whiskers from agglomerated structures, and therefore an estimate of the width of the whiskers was not clearly obtained.

Similarly to the TEM sample preparation, the AFM sample preparation can also lead to nanocrystals aggregated in their images; however, the AFM analysis allows the discernment of individual whiskers of agglomerated structures through transverse height profiles. Thus, the diameter values of CWs obtained from TEM are typically larger than height values obtained from AFM measurements. In addition, detailed structural examination is essential, not only for the CWs manufacturing process developers, but also for the developers of functional applications. In this way, AFM topography measurements were performed for WSH_{30} in order to have a more precise characterization of thickness of the individual crystallites.

Fig. 8 shows the images obtained by AFM. These images also presented needle-like nanoparticles. The average diameter of the WSH_{30} determined by AFM measurements was 2.77 ± 0.67 nm. Fig. 9 shows the histograms corresponding to these measurements. If we consider the diameter obtained by AFM measurements to calculate the aspect ratio for WSH_{30}, this parameter increases markedly, ranging from about 24 up to 77, with an average value of

Table 1
Length, width and aspect ratio, for WSH_{30} and WSH_{40} obtained from TEM analysis.

	Length (nm)	Diameter (nm)	Aspect ratio (nm)
WSH_{30}	122.7 ± 39.40	4.43 ± 1.20	29.41 ± 11.53
WSH_{40}	103.4 ± 29.38	4.36 ± 0.89	24.41 ± 7.10

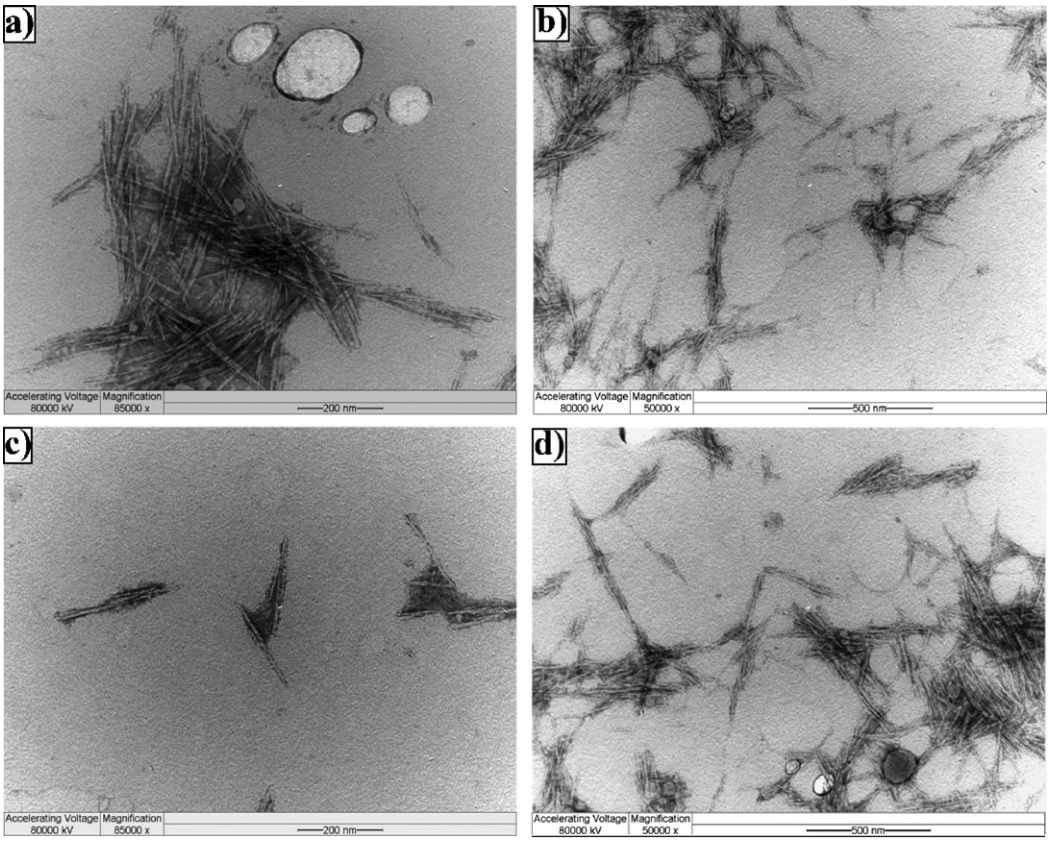

Fig. 6. TEM pictures for cellulose nanocrystals: (a) and (b) extracted at 30 min (WSH_{30}); (c) and (d) extracted at 40 min (WSH_{40}).

about 44, which lies in the range of long nanowhiskers which have great potential to be used as reinforcing agents in nanocomposites (Rosa et al., 2010).

The results of morphological investigation by microscopy-based methods are similar with other reports where CWs were extracted from different sources (Beck-Candanedo et al., 2005; de Rodriguez et al., 2006; Elazzouzi-Hafraoui et al., 2008; Kvien et al., 2005; Rosa et al., 2010; Siqueira et al., 2010; Teixeira et al., 2011).

Determining the exact dimensions of CWs is complicated by the specific limitations of the different analytical methods used. In the case of AFM, tip/sample broadening represents the main limitation, resulting in an overestimation of CWs dimensions. Since the CWs are assumed to be cylindrical in shape, the height of the CWs was taken to be equivalent to the diameter, to compensate for image widening due to the convolution of the tip and the particle (Beck-Candanedo et al., 2005; Kvien et al., 2005). However,

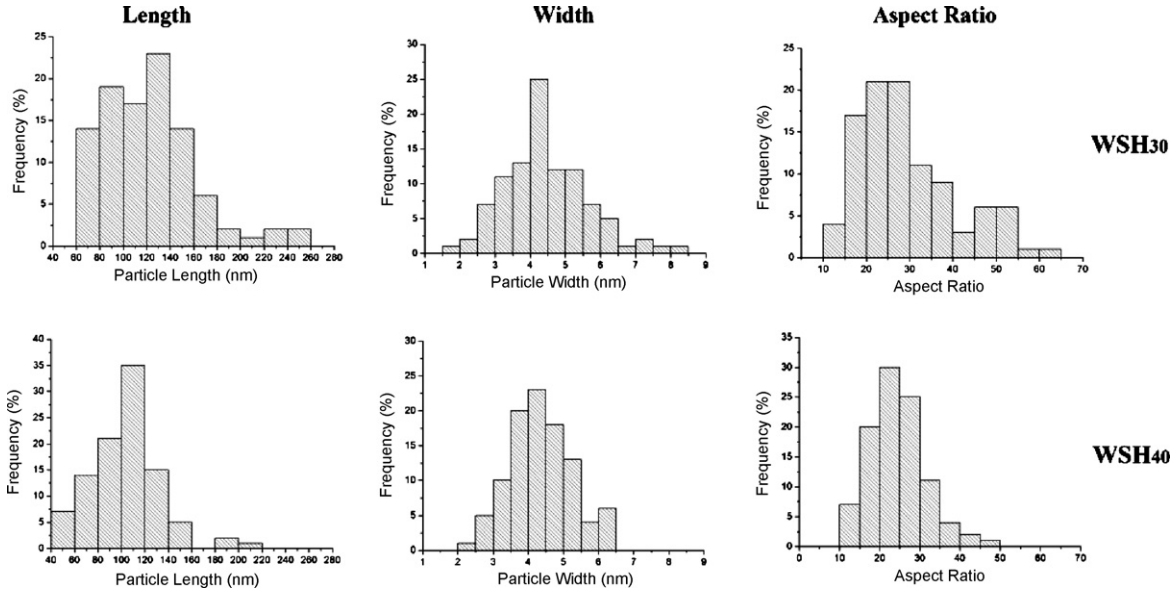

Fig. 7. Length, width and aspect ratio distribution histograms of WSH_{30} and WSH_{40} obtained by TEM micrographs.

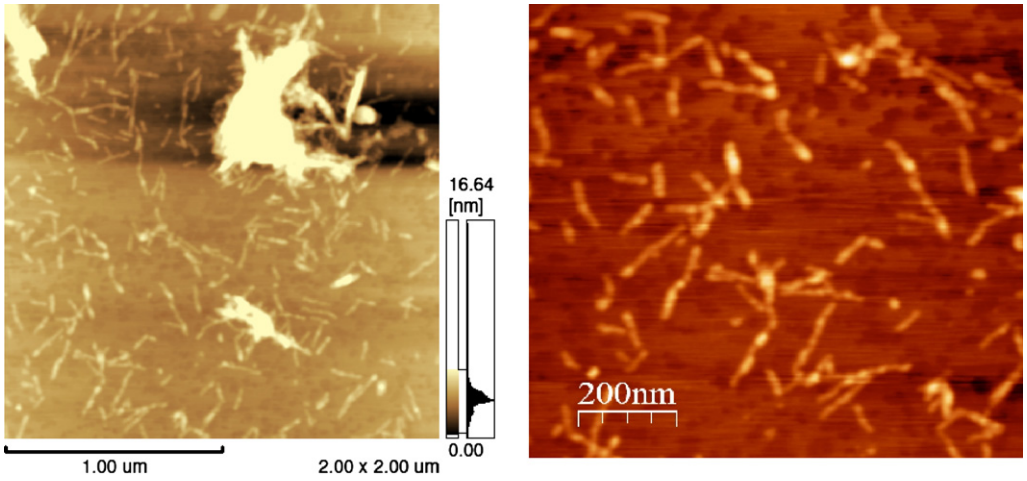

Fig. 8. AFM images of WSH_{30}.

the tip broadening effects causes an error in the length measurements, but this is unavoidable (Beck-Candanedo et al., 2005). On the other hand, detailed information also was obtained by TEM, but this technique required staining and suffered in general from limited contrast and beam sensitivity of the material (Kvien et al., 2005).

An accurate morphological examination can be obtained by TEM and AFM, however, these techniques are restricted to the examination of single particles or a small number of particles in some images. In addition, the information obtained by these techniques requires length times for sample preparation, date collection and data analysis. A measurement of CWs size based on a bulk property, as small- and wide-angle X-ray scattering, would provide a rapid complimentary technique to confirm the results from the above microscopy based methods (Boluk et al., 2011).

The value found for the thickness through the Scherrer's equation is nearest the value found by AFM than by TEM, therefore taking into account what was said in the paragraph above, it is clear that the diameters estimated by TEM did not correspond to individual crystals. Thus, in this case, AFM characterization of thickness is more reliable than TEM.

3.4.3. *Thermogravimetric analysis (TGA)*

As reported in previous studies, the treatment with sulfuric acid leads to a remarkable decrease in thermal stability of cellulose whiskers. Since typical processing temperatures for thermoplastics rise above 200 °C, the thermal stability of these crystals is a key factor in order for them to be used as effective reinforcing materials (Roman and Winter, 2004).

Thermogravimetric (TG) analyses were performed only for SH, TSH and WSH_{30}, because the WSH_{30} has a higher reinforcing capability than WSH_{40}, supported by XRD and TEM analysis. The TG and differential thermogravimetry (DTG) curves of the SH, TSH and WSH_{30} are shown in Fig. 10(A) and (B), respectively. The

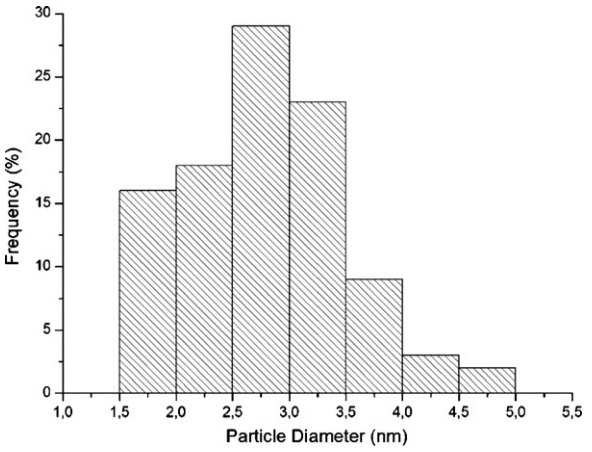

Fig. 9. Diameter distribution histogram of WSH_{30} obtained by AFM measurements.

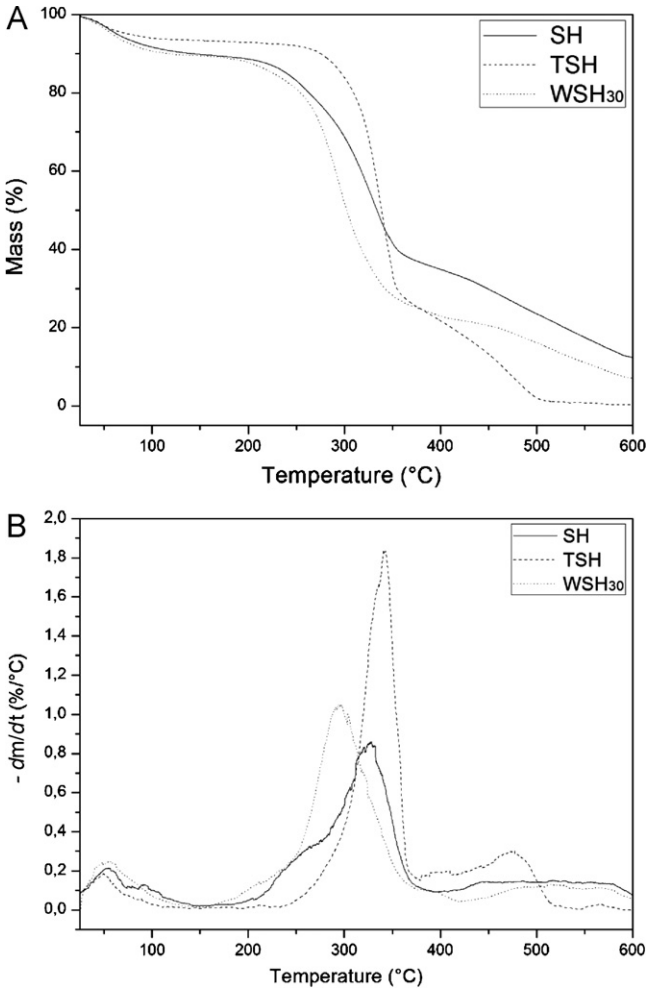

Fig. 10. (A) TG and (B) DTG curves of the SH, TSH and WSH_{30}.

Table 2
Onset temperature (T_{Onset}), degradation temperature on maximum weight-loss rate (T_{Max}), weight loss (WL) and char yield for SH, TSH and WSH_{30} obtained from the TG and DTG curves.

Sample	Water evaporation			Cellulose thermal degradation			Carbonic residue degradation			
	T_{Onset} (°C)	T_{Max} (°C)	WL (%)	T_{Onset} (°C)	T_{Max} (°C)	WL (%)	T_{Onset} (°C)	T_{Max} (°C)	WL (%)	Char yield (%)
SH	25	56	10	190	327	57	420	510	21	12
TSH	25	54	7	240	342	75	423	477	17,5	0,5
WSH_{30}	25	50	10	170	294	68	432	518	15	7

corresponding data are listed in Table 2. In all cases, a small weight loss was found in the range of 35–150 °C, due to the evaporation of the water of the materials or low molecular weight compounds (present in SH).

The first degradation step corresponds basically to cellulose degradation processes such as depolymerization, dehydration and decomposition of glycosyl units (Roman and Winter, 2004). Due to the low decomposition temperature of hemicellulose, lignin and pectin (Morán et al., 2008), the DTG curve of untreated soy hulls showed a small broadening or shoulder on the left side of the main peak, which accounts for the pyrolysis of cellulose (about 340 °C). On the other hand at the same step, the thermal degradation of WSH_{30} also proceeded at lower temperatures than TSH, but this behavior was expected given that the introduction of sulfate groups diminishes the thermostability in the cellulose whiskers because of the dehydration reaction of cellulose crystals as reported elsewhere (Roman and Winter, 2004).

The second degradation step (DTG peak above 425 °C) was attributed to the oxidation and breakdown of the charred residue to lower molecular weight gaseous products (Roman and Winter, 2004). In this step, less charred residue of TSH than that of SH is due to that fact that the non-cellulosic could induce higher char formation (Nguyen et al., 1981), while the increased charred residue of WSH_{30} is because of the sulfate groups acting as the flame retardants (Roman and Winter, 2004). These results are very consistent with results obtained from the chemical composition, XRD and FTIR measurements.

4. Conclusions

The present work shows that cellulose nanocrystals can be isolated from soy hulls. Chemical treatment with sodium chlorite and alkali removed the non-cellulosic constituents resulting in fibers with high content of α-cellulose, hence suitable for extracting CWs. The hydrolysis conditions used led to obtaining stable aqueous suspensions of WSH which are negatively charged, due the presence of sulfate groups. Through the X-ray diffraction was possible to observe that there was formation of cellulose type II in the WSH due to the hydrolysis conditions used permit re-precipitation of cellulose. A longer extraction time (40 min) resulted in a shorter length of WSH and caused some damage on the crystalline structure of cellulose. For extraction time of 30 min the WSH presented a needle-shaped nature, high crystallinity (73.5%), good thermal stability (around 200 °C), an average length (L) of 122.66 ± 39.40 nm, diameter (D) of 2.77 ± 0.67 nm, giving an aspect ratio (L/D) around 44. It can be concluded from these results that the cellulose nanocrystals obtained from soy hulls have great potential to be used as reinforcement agents for the manufacture of nanocomposites. In this study AFM analysis was used as an alternative to electron microscope due to the difficult to judge whether the structures observed in TEM micrographs were individual WSH or several WSH laterally aggregated. The estimated average width of cellulose crystallites by X-ray diffraction patterns through Scherrer's equation is a rapid complimentary technique to confirm the results from the microscopy based methods. In this work a value has been added to an agro-waste material apart from the generation of ecofriendly cellulosic nanofillers for diversified applications.

Acknowledgement

The authors thank CAPES/PROAP, CNPq and FAPEMIG for financial support.

References

Alemdar, A., Sain, M., 2008. Isolation and characterization of nanofibers from agricultural residues – wheat straw and soy hulls. Bioresour. Technol. 99, 1664–1671.
Angellier, H., Putaux, J.L., Boisseau, S.M., Ozil, P., Dufresne, A., 2005. Starch nanocrystal fillers in an acrylic polymer matrix. Macromol. Symp. 221, 95–104.
Azeredo, H.M.C., Mattoso, L.H.C., Wood, D., Williams, T.G., Avena-Bustillos, R.J., McHugh, T.H., 2009. Nanocomposite edible films from mango puree reinforced with cellulose nanofibers. J. Food Sci. 74, N31–N35.
Beck-Candanedo, S., Roman, M., Gray, D.G., 2005. Effect of reaction conditions on the properties and behavior of wood cellulose nanocrystal suspensions. Biomacromolecules 6, 1048–1054.
Boluk, Y., Lahiji, R., Zhao, L., McDermott, M.T., 2011. Suspension viscosities and shape parameter of cellulose nanocrystals (CNC). Colloids Surf. A: Physicochem. Eng. Aspects 377, 297–303.
Borysiak, S., Garbarczyk, J., 2003. Applying the WAXS method to estimate the supermolecular structure of cellulose fibres after mercerization. Fibres Text. East. Eur. 11, 104–106.
Browning, B.L., 1967. Methods of Wood Chemistry, 1st ed. Interscience Publishers, New York.
Chen, Y., Liu, C., Chang, P.R., Cao, x., Anderson, D.P., 2009. Bionanocomposites based on pea starch and cellulose nanowhiskers hydrolyzed from pea hull fibre: effect of hydrolysis time. Carbohydr. Polym. 76, 607–615.
de Rodriguez, N.L.G., Thielemans, W., Dufresne, A., 2006. Sisal cellulose whiskers reinforced polyvinyl acetate nanocomposites. Cellulose 13, 261–270.
Dufresne, A., Caville, J., Vignon, M., 1997. Mechanical behavior of sheets prepared from sugar beet cellulose microfibrils. J. Appl. Polym. Sci. 64, 1185–1194.
Eichhorn, S.J., Dufresne, A., Aranguren, M., Marcovich, N.E., Capadona, J.R., Rowan, S.J., 2010. Review: current international research into cellulose nanofibres and nanocomposites. J. Mater. Sci. 45, 1–33.
Elazzouzi-Hafraoui, S., Nishiyama, Y., Putaux, J.L., Heux, L., Dubreuil, F., Rochas, C., 2008. The shape and size distribution of crystalline nanoparticles prepared by acid hydrolysis of native cellulose. Biomacromolecules 9, 57–65.
Habibi, Y., Lucia, L.A., Rojas, O.J., 2010. Cellulose nanocrystals: chemistry, self-assembly, and applications. Chem. Rev. 110, 3479–3500.
Ipharraguerre, I.R., Clark, J.H., 2003. Soyhulls as an alternative feed for lactating dairy cows: a review. J. Dairy Sci. 86, 1052–1073.
Klug, H.P., Alexander, L.E., 1974. X-ray diffraction procedures for polycrystalline and amorphous materials. Jonh Wiley & Sons, New York.
Kvien, I., Tanem, B.S., Oksman, K., 2005. Characterization of cellulose whiskers and their nanocomposites by atomic force and electron microscopy. Biomacromolecules 6, 3160–3165.
Lima, M.M.S., Borsali, R., 2004. Rodlike cellulose microcrystals: structure, properties, and applications. Macromol. Rapid Commun. 25, 771–787.
Lu, P., Hsieh, Y., 2010. Preparation and properties of cellulose nanocrystals: rods, spheres, and network. Carbohydr. Polym. 82, 329–336.
Moon, R.J., Martini, A., Nairn, J., Simonsen, J., Yougblood, J., 2011. Cellulose nanomaterials review: structure, properties and nanocomposites. Chem. Soc. Rev. 40, 3941–3994.
Morán, J.I., Alvarez, V.A., Cyras, V.P., Vázquez, A., 2008. Extraction of cellulose and preparation of nanocellulose from sisal fibers. Cellulose 15, 149–159.
Nguyen, T., Zavarin, E., Barrall, E.M., 1981. Thermal-analysis of lignocellulosic materials. Part 1. Unmodified materials. J. Macromol. Sci. C: Polym. Rev. 20, 1–65.
Peng, B.L., Dhar, N., Liu, H.L., Tam, K.C., 2011. Chemistry and applications of nanocrystalline cellulose and its derivatives: a nanotechnology perspective. Can. J. Chem. Eng. 89, 1191–1206.
Purkait, B.S., Ray, D., Sengupta, S., Kar, T., Mohanty, A., Misra, M., 2011. Isolation of cellulose nanoparticles from sesame husk. Ind. Eng. Chem. Res. 50, 871–876.
Roman, M., Winter, W.T., 2004. Effect of sulfate groups from sulfuric acid hydrolysis on the thermal degradation behavior of bacterial cellulose. Biomacromolecules 5, 1671–1677.

Rosa, M.F., Medeiros, E.S., Malmonge, J.A., Gregorski, K.S., Wood, D.F., Mattoso, L.H.C., Glenn, G., Orts, W.J., Imam, S.H., 2010. Cellulose nanowhiskers from coconut husk fibers: effect of preparation conditions on their thermal and morphological behavior. Carbohydr. Polym. 81, 83–92.

Segal, L., 1959. An empirical method for estimating the degree of crystallinity of native cellulose using the X-ray diffractometer. Text. Res. J. 29, 786–794.

Shi, J., Shi, S.Q., Barnes, H.M., Pittman Jr., C.U., 2011. A chemical process for preparing cellulosic fibers hierarchically from kenaf bast fibers. Bioresources 6, 879–890.

Siqueira, G., Abdillahi, H., Bras, J., Dufresne, A., 2010. High reinforcing capability cellulose nanocrystals extracted from *Syngonanthus nitens* (Capim Dourado). Cellulose 17, 289–298.

Sun, X.F., Xu, F., Sun, R.C., Fowler, P., Baird, M.S., 2005. Characteristics of degraded cellulose obtained from steam-exploded wheat straw. Carbohydr. Res. 340, 97–106.

Teixeira, E.M., Bondancia, T.J., Teodoro, K.B.R., Corrêa, A.C., Marconcini, J.M., Mattoso, L.H.C., 2011. Sugarcane bagasse whiskers: extraction and characterizations. Ind. Crops Prod. 33, 63–66.

Wang, B., Sain, M., 2007. Isolation of nanofibers from soybean source and their reinforcing capability on synthetic polymers. Compos. Sci. Technol. 67, 2521–2527.

Wang, N., Ding, E., Cheng, R., 2007. Thermal degradation behaviors of spherical cellulose nanocrystals with sulfate groups. Polymer 48, 3486–3493.

Xiang, Q., Lee, Y.Y., Pettersson, P.O., Torget, R.W., 2003. Heterogeneous aspects of acid hydrolysis of α-cellulose. Appl. Biochem. Biotechnol. 107, 505–514.

Zambom, M.A., Santos, G.T., Modesto, E.C., Alcalde, C.R., Gonçalves, G.D., Silva, D.C., Silva, K.T., Faustino, J.O., 2001. Valor nutricional da casca do grão de soja, farelo de soja, milho moído e farelo de trigo para bovinos. Acta Sci. 23, 937–943.